ment processor. Within a matter of minutes, an inspection template made of a stable-base material is ready for use. These templates are used by Quality Assurance to check a finished machined part for proper machining of flanges, webs, and caps by overlaying the FIAT on the machined part. Any deviation from the intended configuration is immediately detectable.

Future Development

The use of CADD has effected many changes in traditional work methods of the various interfacing disciplines at MCAIR. We have streamlined our tasks by utilizing the cost/time saving techniques presently afforded by this system, and plan to continue additional development efforts which will further improve it. As we discover more and more practical applications for CADD, new or modified software routines will be formulated to make the system as responsive and reliable as possible. Since the potential for substantial dollar savings exists, particularly in the area of manufacturing, we are consciously attempting to align our techniques to make engineering data as usable as possible by manufacturing personnel in its existing form, thus eliminating as many intermediate manual processes as possible. Our final objectives, however, cannot now be defined. CADD's utility will increase as we continue to conceive new ideas for its application. Its ultimate benefits can only be determined by the limits of our creative imagination.

DECEMBER 1973 J. AIRCRAFT VOL. 10, NO. 12

Rapid Scanning, Three-Dimensional Hot-Wire Anemometer Surveys of Wing-Tip Vortices

V. R. Corsiglia*
NASA Ames Research Center, Moffett Field, Calif.

R. G. Schwind,† and N. A. Chigier‡
Nielsen Engineering and Research, Inc., Mountain View, Calif.

A rapid-rotation arm traversing mechanism with a three-wire, hot-wire anemometer at the tip was developed for surveying trailing vortices whose paths were distorted over long distances by wind-tunnel turbulence. Measurements were obtained behind two geometrically similar rectangular wings up to 31 span lengths in the Ames 40- by 80-Foot Wind Tunnel. Peak tangential velocities normalized by free-stream velocity and lift coefficient decreased from 0.8 at the trailing edge to 0.6 at 31 span lengths downstream while the circulation within the core remained constant. Measured tangential velocity distributions had the same functional form as that determined by Hoffmann and Joubert.

Nomenclature

A,B,C,D,E	= experimentally determined coefficients of Eqs. (4) to (6)
b	= wing span
c	= wing chord
C_L	= lift coefficient
r	= radial coordinate from vortex center
R_e	= Reynolds number based on c, V_∞
r_0	= outer radius where $\Gamma = 0.99\Gamma_0$
u	= velocity
V_∞	= wind-tunnel mainstream velocity
x	= streamwise ordinate aft from trailing edge
α	= angle of attack, deg
Γ	= circulation around a contour of radius r
Γ_0	= value of circulation shed from one side of wing = $(1/2)C_L V_\infty c$

Subscripts

1	= radius where u_θ is a maximum
max	= maximum value
x	= axial component parallel to vortex axis
θ	= tangential component

Introduction

THERE has been considerable interest in wing-tip trailing vortices from large aircraft because of their danger to smaller following aircraft in the vicinity of airports. Studies that have used wind tunnels have been limited by the relatively short test-section length available since axial distances greater than about 3-span lengths cannot be achieved with a reasonable model scale. The authors have reported previously on the velocity distributions in the wake of a rectangular wing and a CV-990 aircraft model[1,2] at axial distances up to 1.7- and 2.2-span lengths, respectively. Similar measurements have been reported by Mason and Marchman,[3] and Poppleton.[4] El-Ramly[5] has recently compiled a comprehensive survey of the subject.

All previous measurements of velocity distributions in trailing vortices which have been made in wind tunnels were conducted with fixed probes. Generally, the investigators found that trailing vortices were not stationary and that the amplitude of the disturbance increased with distance downstream of the trailing edge. Probes were fixed at a single position, and time mean average values of ve-

Presented as Paper 73-681 at the AIAA 6th Fluid and Plasma Dynamics Conference, Palm Springs, Calif., July 16–18, 1973; submitted July 13, 1973; revision received October 16, 1973.

Index categories: Aircraft Testing (Including Component Wind Tunnel Testing); Viscous Nonboundary-Layer Flows; Research Facilities and Instrumentation.

*Aerospace Engineer. Member AIAA.

†Research Engineer. Member, AIAA.

‡Reader in Chemical Engineering and Fuel Technology, University of Sheffield. Associate Fellow AIAA.

locity were measured. This technique led to errors, particularly near the velocity peaks, depending on the amount of disturbance.

A set of experiments was conducted in the Ames 40- by 80-Foot Wind Tunnel with a ⅓-scale model of the wing used in the earlier experiments in the 7- by 10-Foot Wind Tunnel to obtain greater downstream distances. The maximum downstream distance increased from 1.7- to 31-span lengths. It was recognized at an early stage that measurements with a fixed probe would not be suitable for making velocity traverses in the vortices at far downstream positions. Using the high-frequency response of the hot-wire anemometer and making many high-speed traverses at a fixed axial station and along a fixed lateral path, a series of velocity distributions in the vicinity of the vortex core was obtained as the vortex meandered across the traverse path. By selecting the traverses that came closest to passing through the vortex center, essentially instantaneous velocity profiles were obtained at that particular axial station. Rather than use a linear traversing mechanism that would have involved starting and stopping between traverses, a rotating arm apparatus was constructed which allowed constant speed traverses. The arm radius was made sufficiently large (2.2 m) the the traverse path was essentially linear through the vortex.

The present results using an instantaneous traverse were expected to differ from those of earlier experiments using a fixed probe and time-averaged data at comparable conditions. These differences depend on the shape of the velocity distribution and the time history of the vortex meander. The value of the peak velocities was expected to be lower when the data were averaged. In this regard, Mason and Marchman[3] measured higher peak tangential velocities than did the authors in their earlier work[2] for similar test conditions. Vortex meander is thought to be mainly due to the influence of wind-tunnel turbulence. In Ref. 3, the wind tunnel was equipped with a series of screens designed to minimize turbulence. No such equipment was incorporated in the design of the facility used in Ref. 2.

Apparatus and Procedure

Wings and Strut

A general view of the installation (Fig. 1) shows the wing in the center of the 40- by 80-Foot Wind Tunnel just downstream of the test-section inlet. Table 1 lists dimensions of the wings and strut. The wing tips were square-edged (i.e., a tip fairing was not used). A smoke generator embedded in the wing emitted a dense white smoke (vaporized mineral oil) from the lower surface of the wing tip when desired for flow visualization studies. All plumbing and wiring were entirely contained within the wing

Table 1 Geometric details and test conditions

Wing	
Span, small wing	81 cm (32 in.)
large wing (3× scale)	243 cm (96 in.)
Section	NACA 0015
Aspect ratio	5.33
C_L	0.84, $\alpha = 12°$
	0.56, $\alpha = 8°$
V_∞	2740 cm/sec (90 fps)
Re, small wing	0.3×10^6
Strut	
Thickness	4.8 cm (3.12 in.)
Chord	30.5 cm (12 in.)
Instrument tower	
Rotating arm radius	224 cm (7.34 ft)
Probe tip speed (run)	2740 cm/sec (90 fps)

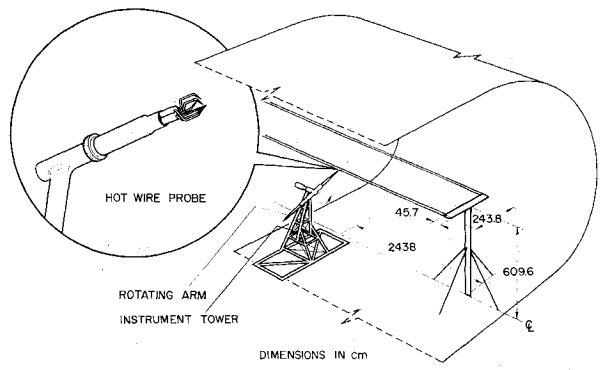

Fig. 1 Instrument tower and rectangular wing in the Ames 40- by 80-Foot Wind Tunnel.

contour. For one test, the wing tip was equipped with a dissipator panel consisting of a flat plate normal to the flow on the wing upper surface (similar to that reported in Ref. 6). Each wing was supported on a very stiff strut of airfoil cross section for minimum interference with the wing flow.

Instrumentation

The measurement probe was supported at the tip of a rotating arm (Fig. 1, Table 1). This rotating arm pivoted on an instrument tower that could be remotely positioned laterally in the wind tunnel along guide rails at its base. The arm was driven by an electric motor at about 2.0 rps during a run. The probe was a commercially available, triple sensor hot wire consisting of three wires in an orthogonal array. The probe and anemometry were identical to those used earlier.[1,2] The circumferential speed of the probe was set equal to the tunnel speed so that, with the probe aligned 45° to the tunnel centerline, the relative flow was parallel to the probe axis when the probe was outside the vortex. Signals from the hot wires passed through slip rings to anemometers outside the wind tunnel. The anemometer output was monitored on d.c. voltmeters and passed through a high-pass filter (set at 5 Hz) to record only the a.c. component of the siganl on an analog tape. These analog signals were subsequently copied on a digital tape for data reduction.

Calibration Procedure

The anemometers were calibrated immediately before each run by setting several tunnel speeds equal to the probe speed and recording the d.c. voltage with the instrument tower located so that the vortex was not traversed by the probe. The data were then processed by fitting the King's Law equation. The sensitivity of the calibration to the tunnel temperature was minimized by using a temperature compensation probe in the flow near the point where the velocities were recorded. The recording system was calibrated on each reel of tape by replacing the anemometer output with a known sine wave and processing this signal.

Run Procedure

For flow visualization tests smoke was generated from the wing tip and movie films were taken of the smoke which quickly spiraled in close to the core. These films were analyzed to show vortex location in the wind tunnel as a function of time (Fig. 2). Smoke studies were completed and the smoke was shut off before calibration to prevent contamination of the hot wires. A run to obtain hot wire anemometer data consisted in initially setting the test conditions with the tower at a fixed axial and lat-

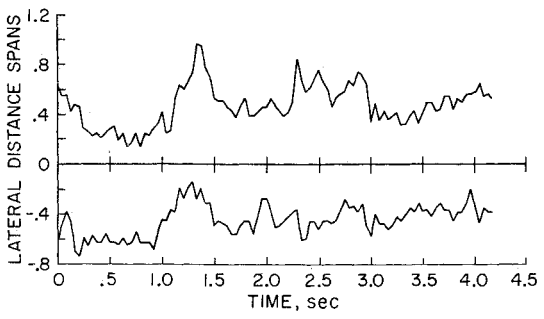

Fig. 2 Vortex meander; location of vortex centers as function of time.

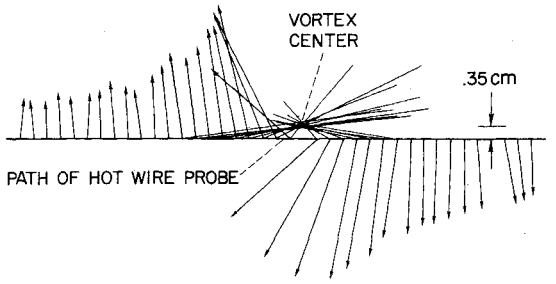

Fig. 4 Vector construction from velocity components measured along probe traverse path as used to determine vortex center and tangential velocity.

eral position and observing the anemometer output on an oscilloscope. The encounter of the probe with the vortex could be clearly discerned, so a lateral position was selected to maximize the frequency of vortex core penetrations. The positions determined in this manner were found to agree with visual observations of the vortex as marked by smoke. Run data were recorded continuously for about 4 min to ensure that many vortex core penetrations were encountered. Only the core penetration traverses were digitized for further analysis.

Velocity Distributions

Three components of velocity were obtained by applying the hot-wire calibration to the combination of the a.c. and d.c. components of the anemometer signal to determine the velocities normal to each wire. From these velocities, three velocity components in a coordinate system fixed to the orthogonal wire array were determined using the known geometry of the array. These velocity components were then transformed to a nonrotating coordinate system. The components of velocity relative to the vortex center were determined by a graphical procedure (discussed later) that yielded the location of the traverse relative to the vortex center.

Results

Meander

The spanwise location of the two vortices (as determined from frame-by-frame analysis of movie films), using smoke for visualization, is shown in Fig. 2 for a typical time segment. Analysis[7] showed no dominant frequency characterizes the meander. The spectrum of the power of the vortex motion had a characteristic typical of isotropic turbulence. It was concluded that meander is the result of wind-tunnel turbulence. The amplitude of the disturbances is related through theoretical considerations to the scale of turbulence in the wind tunnel in Ref. 7.

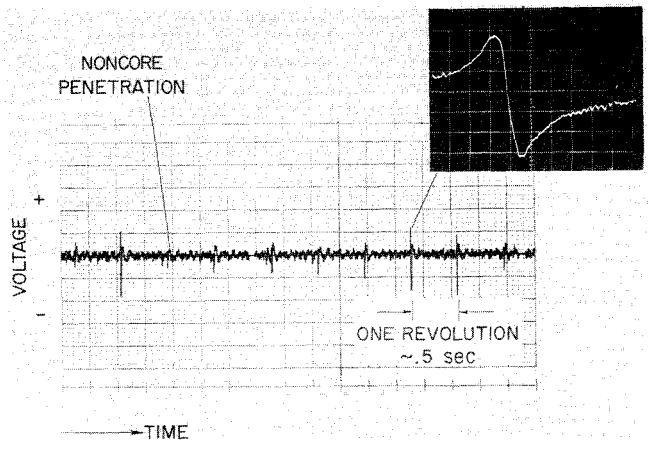

Fig. 3 Continuous trace of output from hot-wire anemometer showing core and noncore penetrations.

Traces of Hot-Wire Signals

The continuous trace of the output from one hot-wire anemometer (Fig. 3) indicates high-amplitude signals when the vortex core was intersected and lower-amplitude signals when the traverse passed some distance from the core. The inset in Fig. 3 shows a single vortex core traverse, in expanded scale, as recorded on an oscilloscope. This signal shows the two distinct peaks with a linear core region. Furthermore, there appears to be higher turbulence in the region outside the peak velocities while the core region gives the appearance of laminar-like flow. It is apparent from the sequence of traces that all the vortex encounters are not identical. This is mainly caused by different relative positions between the probe and the vortex center due to vortex meander.

Tangential Velocity

The varying relative position between each traverse and the vortex center was obtained from a vector construction using velocity components measured along the probe traverse path as shown in Fig. 4. The tangential velocity and radial distance were obtained for each run from the result. Measurements from three separate traverses, selected from several hundred as being close to the vortex center, are shown in Fig. 5 for one downstream distance and angle of attack. Some time-dependent variation in vortex velocities was noted. Only those profiles which produced the highest velocities were considered for further analysis.

Prediction of Turbulent Vortex

Nielsen and Schwind[8] have described turbulent vortices based on an analogy with turbulent boundary layers. They divided the vortex into three regions: the inner or core region, analogous to the laminar sublayer; a logarithmic region where the circulation distribution is logarithmic, analogous to the law of the wall; and an outer region where a defect law applies, analogous to the outer region of a turbulent boundary layer.

The equations used by Nielsen and Schwind, based on the data of Hoffmann and Joubert,[9] are

Core region:

$$\Gamma/\Gamma_1 = 1.83(r/r_1)^2 \quad (1)$$

Logarithmic region:

$$\Gamma/\Gamma_1 = 0.928 \ln(r/r_1) + 1 \quad (2)$$

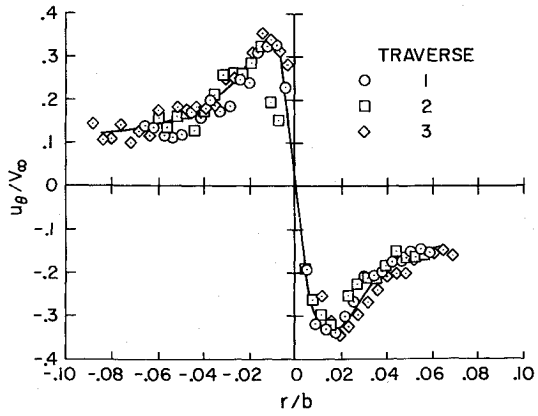

Fig. 5 Tangential velocity distribution; b = 81 cm, α = 8°, x/b = 31.

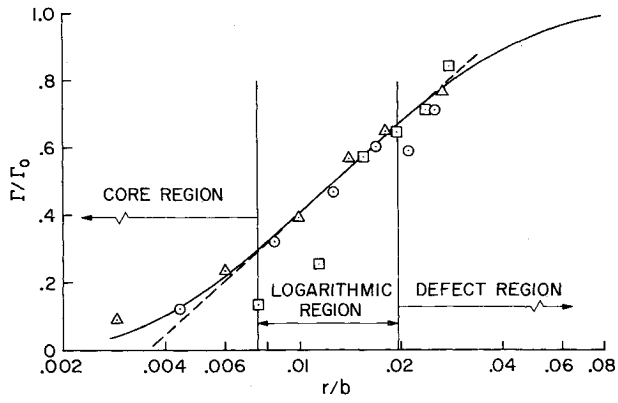

Fig. 6 Circulation distribution in logarithmic region.

Defect region:

$$(\Gamma_0 - \Gamma)/\Gamma_1 = 4.43e^{-4.8r/r_0} \quad (3)$$

To use these expressions for prediction purposes, the values of Γ_1, r_1, and r_0 must be known. Because of the small core radius and sharp velocity peak, it is difficult to ascertain very accurately the exact magnitude and location of the maximum tangential velocity. Furthermore, since Γ approaches Γ_0 in the outer region asymptotically, where velocity magnitudes are low and approach the lower limits of instrument capability, the radius r_0 is also difficult to determine accurately. Therefore, from the practical point of view of attempting to fit measured data to a set of expressions containing constants, it is more appropriate to rewrite Eqs. (1–3) as follows:

Core region:

$$\Gamma/\Gamma_0 = A(r/b)^2 \quad (4)$$

Logarithmic region:

$$\Gamma/\Gamma_0 = B \ln(r/b) + C \quad (5)$$

Defect region:

$$\ln[1 - (\Gamma/\Gamma_0)] = D(r/b) + E \quad (6)$$

In Eqs. (4) to (6), Γ_0 is selected for nondimensionalizing Γ_0 since it can be readily calculated from the wing lift coefficient, vortex spacing, and freestream velocity. The terms Γ_1 and r_1 can be obtained from Eq. (5)

$$\left.\begin{aligned}\Gamma_1/\Gamma_0 &= B \\ r_1/b &= e^{(1-C/B)}\end{aligned}\right\} \quad (7)$$

The circulation distribution in the logarithmic region for a typical condition is shown in Fig. 6 from which the values of the coefficients in Eq. (5) were determined. All the measured data fit a logarithmic distribution in the range $0.008 < r/b < 0.02$. The circulation distribution in the defect region, however, is difficult to obtain using a semilogarithmic plot of $(1 - \Gamma/\Gamma_0)$ versus r/b because of the scatter that is accentuated in this form. As the outer regions of the vortex are approached, the vortex is more sensitive to ambient turbulence and more scatter would be expected. We can expect high local turbulence intensity values as well as intermittency between laminar and turbulent flow for the turbulent vortex, as is generally found in the outer regions of jets and wakes. The values of constants D and E in Eq. (6) were obtained to give the best fit of tangential velocity. Figure 7 shows a typical comparison of the present tangential velocity measurements with the functional form of Eqs. (4–6).

The present measurements using hot-wire anemometry, as well as those by Mason and Marchman[3] using a pressure probe and by Lezius[10] using the hydrogen bubble technique, yield the same functional form of the tangential velocity. Orloff and Grant[11] note some difficulty with this functional form for small downstream distance. It is expected, however, that the form is applicable only beyond sufficient downstream distance to achieve an equilibrium profile.[9] Also, the rectangular wings that have been used have nearly rectangular span loading, which leads to a very rapid rollup of the vortex sheet. Wings with span loadings of a more elliptical shape are expected to require greater downstream distance before the Hoffmann and Joubert profile is valid. It appears then that all that is required from experiments, where an equilibrium profile has been achieved, is to establish values for the constants in Eqs. (4–6). The values of these constants for the present experiments are shown in Table 2.

The constants A–E depend on the wing configuration, the downstream distance, and, possibly, on the turbulence characteristics of the flow between the generating wing and the downstream point being considered. Table 2 shows the magnitude of this dependance for variations of angle of attack, downstream distance and dissipator panel (discussed later). The effect of freestream turbulence was not included in the present investigation and is a subject for future research. Also the effects of vortex bursting have not been determined. Vortex bursting was not observed over the downstream distances included in this investigation.

Prediction of Inviscid Vortex

Rossow[12] improved the theory of Betz[13] by deriving a new form of the rollup relationship. Betz' theory assumes

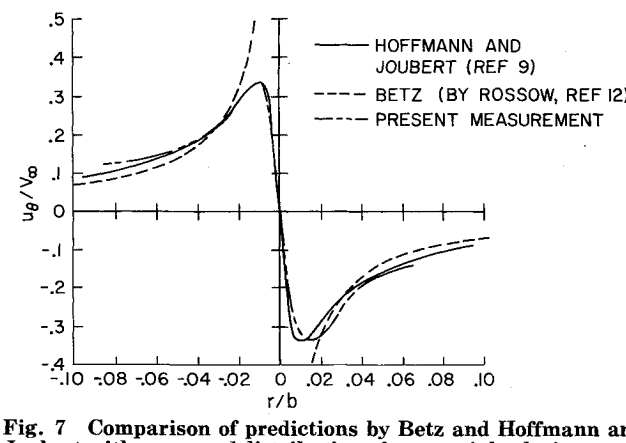

Fig. 7 Comparison of predictions by Betz and Hoffmann and Joubert with measured distribution of tangential velocity.

Table 2 Constants A and E measured from data [see Eqs. (4)–(6)].

Wing	Span, cm	α	x/b	$A \times 10^{-4}$	B	C	D	E
Clean	81	8	10	0.57	0.42	2.35	−40.8	−0.372
Clean	81	8	31	0.54	0.40	2.24	−44.7	−0.265
Clean	81	12	5	0.79	0.42	2.42	−55.8	−0.458
Clean	81	12	10	0.65	0.45	2.53	−70.1	+0.070
Clean	81	12	24	0.55	0.46	2.54	−83.5	+0.262
Dissipator	243	8	10	0.084	0.47	2.16	−32.2	+0.328
Clean	243	12	10	0.61	0.44	2.48	−19.2	−0.704
Average value					0.44			

that 1) the flowfield is two-dimensional, inviscid, and incompressible with no variation in streamwise velocity, 2) half the vortex sheet is isolated from the other half so that the developed vortex is axially symmetric, and 3) the rollup of vorticity from the sheet into the vortex is orderly and sequential. Rossow predicted the velocity distribution for the wing used in the present experiments using the previously measured span-load distribution[1]; the result is shown in Fig. 7.

Since the Betz prediction is for inviscid flow, it is not possible to predict the core radius or the maximum tangential velocity. Reasonable agreement is shown between the Betz prediction and the measured values in the outer region, but the predicted values are much greater than the measurements in the core and logarithmic regions.

Secondary Vortices

Secondary vortices contained within the main vortex or precessing around the main vortex axis have been reported in the past.[14,15] The traces of the voltage output from the hot-wire anemometer occasionally showed the presence of a secondary vortex for runs made at axial stations closest to the wing. The tangential velocity profile in Fig. 8 shows the presence of a secondary vortex. The secondary vortex appeared for the three traverses that were analyzed at this downstream distance and angle of attack.

Secondary vortices would be expected to be shed from the wing at locations of abrupt changes in span loading or at the locations of a shedding boundary layer. The wing tip in the present study was blunt which resulted in a shed vortex similar to the leading edge vortex on a sharp-edged delta wing. This shed vortex passed over the wing upper surface near the tip and reduced the upper surface pressures.[1] It is possible that this shed vortex from the blunt wing tip has remained distinct from the main vortex for 5-span lengths downstream and explains the secondary vortex shown on Fig. 8. Ultimately the secondary vortex would be expected to diffuse into the main vortex. The reason that the secondary vortex did not appear at the more aft stations of this study could be that this diffusion has taken place or the secondary vortex has moved to an azimuth off the traverse path.

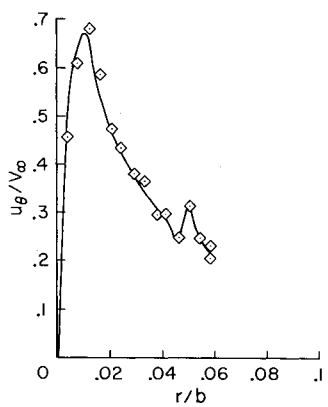

Fig. 8 Presence of a secondary vortex; b = 81 cm, α = 12°, x/b = 5.

Variation With Axial Distance

The variation of vortex parameters with axial distance downstream of the wing is important in assessing the potential hazard of following aircraft that encounter trailing vortices. The variation of core radius normalized with the span and maximum tangential velocity normalized with tunnel speed and lift coefficient are shown in Fig. 9. The data presented include 8° and 12° wing angle of attack, as well as two geometrically similar models with 81- and 243-cm wing spans, respectively. There is no effect of angle of attack on the dimensionless velocity or core radius. This result agrees with results reported by McCormick et al.,[16] the present authors,[2] and Orloff and Grant,[11] where the peak tangential velocity was found to be proportional to the lift coefficient for a clean rectangular wing. The limited tests using the larger (243 cm) span wing indicate no effect of scale on the dimensionless core radius or peak tangential velocity.

The core radius increases with downstream distance while the peak tangential velocity decreases. The data are shown to be reasonably faired such that the product of core radius and peak tangential velocity is constant. This implies that the circulation within the core region is constant. This same result is shown in Table 2, where the constant B, which is proportional to the core circulation [Eq. (7)], shows little variation from the average for the conditions tested. These results suggest a possible universality of the constant B in the Hoffmann and Joubert formulation.

The dimensionless peak tangential velocity decreases from $u\theta_{max}/(V_\infty)(C_L) = 0.8$ at the wing trailing edge to 0.6 at 31-span lengths downstream. Measurements[11] made with a laser anemometer in the near flowfield correlate well with the present hotwire measurements. Measurements by Mason and Marchman[3] using a pressure probe in a low-turbulence wind tunnel are lower in core radius and velocity than those of the present authors and Orloff. This lower velocity could possibly be ascribed to the effects of averaging in the presence of vortex meander.

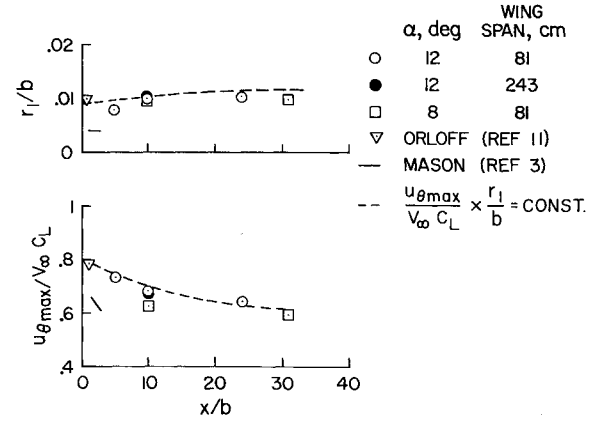

Fig. 9 Variation of maximum tangential velocity and core radius with downstream distance.

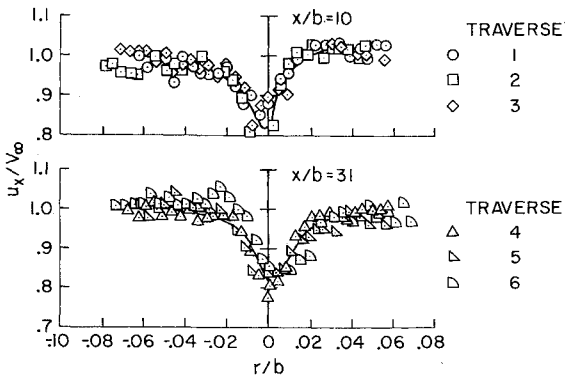

Fig. 10 Distributions of axial velocity at x/b = 10 and 31, α = 8°.

Measured profiles of axial velocity are shown in Fig. 10 for x/b = 10 and 31. The profiles show an axial velocity defect with a peak value ux_{max}/V_∞ = 0.8 and no significant variation with downstream distance.

Dissipator Panel

The substantial reductions in tangential velocity with corresponding increases in core dimensions obtained by introducing a dissipator panel at the wing tip (reported previously by the authors[6]) were confirmed in the present tests. Tangential velocity profiles at α = 8° and x/b = 10 are shown in Fig. 11. Circulation distributions for the vortex with the dissipator panel installed fit expressions (4–6). The empirical constants for this case are given in Table 2. The profile with the dissipator panel installed can therefore be taken to be equivalent to that expected from a vortex from a clean wing but with greater age.

If an aircraft flies parallel to the trailing vortex of the aircraft ahead, it experiences a rolling moment due to the swirling flow of the trailing vortex. The magnitude of this rolling moment was estimated, using a strip lift theory, for the case of the following aircraft aligned with the trailing vortex center. It was found that the effect of the dissipator was to reduce the induced rolling moment on the trailing aircraft 30% for a span ratio (follower/generator) of 0.2. However, the induced rolling moment for this case would be about 2.5 to 5 times the rolling moment control capability of a typical trailing aircraft, depending on the speed of the follower.

Conclusions

The feasibility of measuring instantaneous velocity distributions in vortices undergoing significant meander has been demonstrated by using a three-dimensional, hot-wire probe mounted on a rotating arm in the Ames 40- by 80-Foot Wind Tunnel.

Magnitudes of tangential velocity measured with the rapid-scanning, hot-wire anemometer agree with those made by Orloff using a laser anemometer. Earlier measurements[3] of maximum velocity using a pressure probe, as well as those by the authors with a hot wire (both involved time averaging), were lower than those obtained in the present study.

Measured tangential velocity distributions had a functional form that could be fit by the one determined by Hoffmann and Joubert. The empirical equations based on the data of Hoffmann and Joubert have been modified so that circulation is normalized by the initial wing circulation and radial distance is normalized by the wing span. The values of the empirical constants in the modified equations have been determined for two rectangular wings

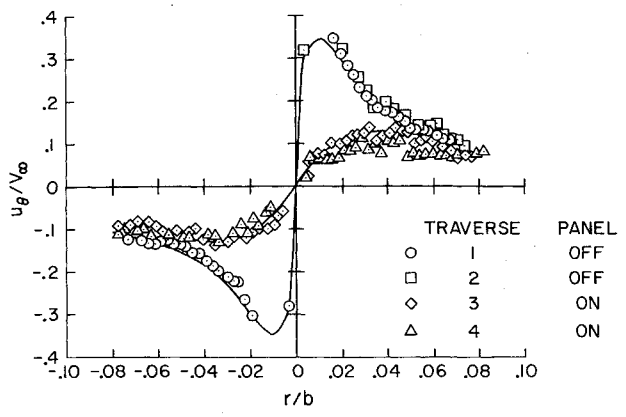

Fig. 11 Effect of a dissipator panel on the tangential velocity distribution α = 8°, x/b = 10, b = 243 cm.

at 8° and 12° angle of attack and at downstream distances up to 31 spans.

Over the range $0 < x/b < 31$ maximum tangential velocities, $u\theta_{max}/(V_\infty)(C_L)$ were reduced from 0.8 to 0.6, while circulation in the core remained constant.

Measured axial velocities reached values u_x/V_∞ = 0.8 with no appreciable downstream variation.

References

[1]Chigier, N. A. and Corsiglia, V. R., "Tip Vortices—Velocity Distributions," TM X-62 087, Sept. 1971, NASA.

[2]Chigier, N. A. and Corsiglia, V. R., "Wind-Tunnel Studies of Wing Wake Turbulence," *Journal of Aircraft*, Vol. 9, No. 12, Dec. 1972, pp. 820–825.

[3]Mason, W. H. and Marchman, J. F., "Farfield Structure of an Aircraft Trailing Vortex, Including Effects of Mass Injection," CR-62078, 1972, NASA.

[4]Poppleton, E. C., "A Preliminary Investigation of the Structure of a Turbulent Trailing Vortex," TN 71-1, March 1971, McGill Univ., Montreal, Canada.

[5]El-Ramly, Z., "Aircraft Trailing Vortices, A Survey of the Problem," Rept. ME/A72-1, Nov. 1972, Carleton Univ., Ottawa Canada.

[6]Corsiglia, V. R., Jacobsen, R. A., and Chigier, N. A., "An Experimental Investigation of Trailing Vortices Behind a Wing With a Vortex Dissipator," *Aircraft Wake Turbulence and Its Detection*, edited by J. Olson, A. Goldberg, and M. Rogers, Plenum Press, New York, 1971 pp. 229–242.

[7]Reed, R. E., Jr., "Properties of the Lateral Random Oscillations of Trailing Vortices Observed in Wind-Tunnel Tests," TR 47, Jan. 1973, NEAR, Inc., Mountain View, Calif.

[8]Nielsen, J. N. and Schwind, R. G., "Decay of a Vortex Pair Behind an Aircraft," *Aircraft Wake Turbulence and Its Detection*, edited by J. Olson, A. Goldberg, and M. Rogers, Plenum Press, New York, 1971, pp. 413–454.

[9]Hoffmann, E. R. and Joubert, P. N., "Turbulent Line Vortices," *Journal of Fluid Mechanics*, Vol. 16, Pt. 3, July 1963, pp. 395–411.

[10]Lezius, D. K., "Study of the Far Wake Vortex Field Generated by a Rectangular Airfoil," TM X-62,274, May 1973, NASA.

[11]Orloff, K. L. and Grant, G. R., "Application of a Scanning Laser Doppler Velocimeter to Trailing Vortex Definition and Alleviation," TM X-62,243, Feb. 1973, NASA.

[12]Rossow, V. J., "On the Inviscid Rolled-Up Structure of Lift-Generated Vortices," TM X-62,224, 1973, NASA.

[13]Betz, A., "Behavior of Vortex Systems," TM-713, 1933, NACA.

[14]Caiger, B. and Gould, D. B., "An Analysis of Flight Measurements in the Wake of a Jet Transport Aircraft," *Aircraft Wake Turbulence and Its Detection*, edited by J. Olsen, A. Goldberg, and M. Rogers, Plenum Press, New York, 1971, pp. 125–135.

[15]Kuhn, G. D. and Nielsen, J. N., "Analytical Studies of Aircraft Trailing Vortices," Paper No. 20, Jan. 1972, NEAR, Inc., Mountain View, Calif.

[16]McCormick, B. W., Tangler, J. L., and Sherrieb, H. E., "Structure of Trailing Vortices," *Journal of Aircraft*, Vol. 5, No. 3, March 1968, pp. 260–267.